Transferability Between Regression Tasks

Anonymous authors
Paper under double-blind review

Abstract

We consider the problem of estimating how well deep neural network regression models would transfer from source to target tasks. We focus on regression tasks, which received little previous attention, and develop novel transferability estimation methods that are simple, computationally efficient, yet effective and theoretically grounded. We propose two families of transferability estimators, both of which utilize the mean squared error of a regularized linear regression model to estimate the transferability. We prove novel theoretical bounds connecting our methods with the expected risk of the optimal target models obtained from the actual transfer learning process. We test our methods extensively in various challenging, practical scenarios and show they significantly outperform existing state-of-the-art regression task transferability estimators, in both accuracy and efficiency.

1 Introduction

We consider the problem of transferability estimation (Bao et al., 2019; Tran et al., 2019; Nguyen et al., 2020): Deriving computationally efficient metrics to predict the effectiveness of transferring a deep learning model from source to target tasks. This problem has recently gained attention as a means for model and task selection (Bao et al., 2019; Tran et al., 2019; Nguyen et al., 2020; Bolya et al., 2021; You et al., 2021) that can potentially improve the performance and reduce the cost of transfer learning, especially for expensive deep learning models. In recent years, new transferability estimators were also developed and used in other applications such as checkpoint ranking (Huang et al., 2021; Li et al., 2021) and few-shot learning (Tong et al., 2021).

Nearly all existing methods consider only the transferability of classification tasks (Bao et al., 2019; Tran et al., 2019; Nguyen et al., 2020; Deshpande et al., 2021; Li et al., 2021; Tan et al., 2021; Huang et al., 2022) with very few designed to estimate transferability of regression models (You et al., 2021; Huang et al., 2022). Regression problems are as important as classification problems and include applications such as landmark detection (Fard et al., 2021; Poster et al., 2021), object detection and localization (Cai et al., 2020; Bu et al., 2021), pose estimation (Schwarz et al., 2015; Doersch & Zisserman, 2019), and music tagging (Choi et al., 2017; Manco et al., 2022). Despite their importance, however, those few methods proposed for estimating regression model transferability have so far been either complex and inefficient (You et al., 2021) or ineffective (Huang et al., 2022), as we will show in our experiments. Those methods also do not have theoretical insights into the performance of the transferred target model.

Compared to previous work, we offer *efficient and theoretically grounded* transferability estimation for regression problems. We propose to use two families of very simple transferability estimators, which utilize the penalized mean squared error (MSE) of a regularized linear regression model computed from the source and target training sets. The first family, called *Linear MSE*, estimates the transferability by regressing between features extracted from a model trained on the source task (the *source model*) and true labels of the target training set. The second family, *Label MSE*, estimates transferability by regressing between the *dummy* labels, obtained from the source model, and true labels of the target data. In special cases where the source and target training sets share the inputs, the Label MSE estimators can be computed efficiently from the two label sets without requiring a source model.

In addition to their simplicity, our methods can be shown to have theoretical properties in terms of generalization bounds on the expected risk (or true risk) of the transferred target model. In particular, we can prove that the expected risk of the target model obtained from the actual transfer learning process is upper bounded by the Label MSE plus a complexity term, which depends on the target dataset size and the architecture of the neural network model. Similar results can also be proven for the case where the source and target datasets share the input set.

We conduct extensive experiments on two real-world keypoint detection datasets, CUB-200-2011 (Wah et al., 2011) and OpenMonkey (Yao et al., 2021), as well as the dSprites shape regression dataset (Matthey et al., 2017) to show the advantages and usefulness of our proposed methods. Our results clearly demonstrate that the proposed methods outperform recently published, state-of-the-art (SotA) transferability estimators for regression problems, such as LogME (You et al., 2021) and TransRate (Huang et al., 2022), in both effectiveness and efficiency.

Summary of contributions. We make the following contributions: (1) We propose two simple yet effective families of transferability estimators between regression tasks. (2) We prove novel theoretical properties for these methods, including generalization bounds for the expected risk of the target models. (3) We rigorously test our methods in various experimental settings and challenging benchmarks, showing our advantages compared to SotA regression transferability methods.

2 TRANSFERABILITY BETWEEN REGRESSION TASKS

In this section, we describe the formal transfer learning setting for regression tasks and propose two families of transferability estimators for this setting. The estimators are both simple and intuitive, allowing us to show their theoretical properties as well as their empirical superiority compared to previous methods.

2.1 TRANSFER LEARNING BETWEEN TWO REGRESSION TASKS

Consider a source training set $\mathcal{D}_s = \{(x_i^s, y_i^s)\}_{i=1}^{n_s}$ and a target training set $\mathcal{D}_t = \{(x_i^t, y_i^t)\}_{i=1}^{n_t}$ consisting of n_s and n_t examples respectively, where $x_i^s, x_i^t \in \mathbb{R}^d$ are d-dimensional input vectors, $y_i^s \in \mathbb{R}^{d_s}$ is a d_s-dimensional source label vector, and $y_i^t \in \mathbb{R}^{d_t}$ is a d_t-dimensional target label vector, for all i. Note that we allow multi-output regression tasks (i.e., $d_s, d_t \geq 1$) where the source and target label vectors may have different dimensions (e.g., $d_s \neq d_t$). In the simplest case, the source and target tasks are both single-output regression tasks, i.e., $d_s = d_t = 1$.

From the source dataset $\mathcal{D}_s$, we train a deep learning model (w^*, h^*) consisting of an optimal feature extractor w^* and an optimal regression head h^* that minimizes the empirical MSE loss:

$$w^*, h^* = \operatorname*{argmin}_{w,h} \mathcal{L}(w, h; \mathcal{D}_s), \tag{1}$$

where $w : \mathbb{R}^d \to \mathbb{R}^{d_r}$ is a feature extractor network that transforms a d-dimensional input vector into a d_r-dimensional feature vector, $h : \mathbb{R}^{d_r} \to \mathbb{R}^{d_s}$ is a source regression head network that transforms a d_r-dimensional feature vector into a d_s-dimensional output vector, and $\mathcal{L}(w, h; \mathcal{D}_s)$ is the empirical MSE loss of the whole model (w, h) on the dataset $\mathcal{D}_s$:[1]

$$\mathcal{L}(w, h; \mathcal{D}_s) = \frac{1}{n_s} \sum_{i=1}^{n_s} \|y_i^s - h(w(x_i^s))\|^2, \tag{2}$$

with $\|\cdot\|$ being the ℓ_2 norm. In practice, we usually consider a source model as a whole (e.g., a ResNet model (He et al., 2016)) and use its first l layers from the input (for some chosen number l) as the feature extractor w. The regression head h is the remaining part of the model from the l-th layer to the output layer, and the prediction for any input x is $h(w(x))$.

After training the optimal source model (w^*, h^*), we perform transfer learning to the target task by freezing the optimal feature extractor w^* and re-training a new regression head k^* using the target dataset $\mathcal{D}_t$, also by minimizing the empirical MSE loss:

$$k^* = \operatorname*{argmin}_{k} \mathcal{L}(w^*, k; \mathcal{D}_t) = \operatorname*{argmin}_{k} \Big\{ \frac{1}{n_t} \sum_{i=1}^{n_t} \|y_i^t - k(w^*(x_i^t))\|^2 \Big\}, \tag{3}$$

where $k : \mathbb{R}^{d_r} \to \mathbb{R}^{d_t}$ is a target regression head network that may have a different architecture than that of h. In general, the regression heads h and k may contain multiple layers and are not

[1]In this paper, we refer to a model (such as w, w^*, h, h^*, k, or k^*) and its parameters interchangeably.

necessarily linear. The transfer learning setting described here has been widely used for deep learning models (Donahue et al., 2014; Oquab et al., 2014; Sharif Razavian et al., 2014; Whatmough et al., 2019). This setting, usually called *head re-training*, will be used for the theoretical analysis of our transferability methods. However, in practice and in our experiments, we also consider another transfer learning setting, widely known as *fine-tuning*, where we fine-tune the trained feature extractor w^* on the target set, and then train a new target regression head k^* with this fine-tuned feature extractor (Agrawal et al., 2014; Girshick et al., 2014; Chatfield et al., 2014; Dhillon et al., 2020).

2.2 Transferability Estimators

A transferability estimator measures the effectiveness of transfer learning given a pair of source and target tasks. Intuitively, we can use $\mathcal{L}(w^*, k^*; \mathcal{D}_t)$, the MSE of the transferred target model, as an estimator. However, computing $\mathcal{L}(w^*, k^*; \mathcal{D}_t)$ means that we need to run the actual transfer learning process, which could be expensive if the network architecture of the target regression heads (e.g., k and k^*) is deep. A simple way to reduce this computational cost is to approximate $\mathcal{L}(w^*, k^*; \mathcal{D}_t)$ using an ℓ_2 regularized linear regression (or Ridge regression) head; that is, we consider the family of *Linear MSE* estimators below. In our definitions, $\|\cdot\|_F$ is the Frobenius norm.

Definition 1 (Linear MSE). *A Linear MSE transferability estimator between a source dataset $\mathcal{D}_s$ and a target dataset $\mathcal{D}_t$, with a regularization parameter $\lambda \geq 0$, is defined as: $\mathcal{T}_\lambda^{\text{lin}}(\mathcal{D}_s, \mathcal{D}_t) := \min_{A,B} \left\{ \frac{1}{n_t} \sum_{i=1}^{n_t} \|y_i^t - Aw^*(x_i^t) - B\|^2 + \lambda \|A\|_F^2 \right\}$, where $A \in \mathbb{R}^{d_r \times d_t}$ is a $d_r \times d_t$ real-valued matrix and $B \in \mathbb{R}^{d_t}$ is a d_t-dimensional real-valued vector.*

We add a regularizer to the estimator to avoid overfitting when the target dataset $\mathcal{D}_t$ is small. Previous work such as LogME (You et al., 2021) proposed to prevent overfitting by taking a Bayesian approach, which is more complicated and expensive. In this paper, we argue that a simple regularization approach can tackle the issue effectively and more efficiently.

Given a pre-trained feature extractor w^* and a target dataset $\mathcal{D}_t$, we can compute $\mathcal{T}_\lambda^{\text{lin}}(\mathcal{D}_s, \mathcal{D}_t)$ efficiently using the closed form solution for Ridge regression or using second-order optimization. If the target regression head is restricted to only linear regression model, $\mathcal{T}_0^{\text{lin}}(\mathcal{D}_s, \mathcal{D}_t)$, the Linear MSE without regularization, is equal to the MSE of the transferred target model (w^*, k^*) on $\mathcal{D}_t$. If the target regression head has more than one layer with a non-linear activation function, $\mathcal{T}_\lambda^{\text{lin}}(\mathcal{D}_s, \mathcal{D}_t)$ can be regarded as using a regularized linear model to approximate this non-linear head.

Although the Linear MSE transferability score above can be computed efficiently, this computation may still be expensive if the feature vectors $w^*(x_i^t)$ are high-dimensional. Furthermore, in many cases, we need to compute and compare the scores for several pairs of datasets, resulting in high computational costs. To further reduce the costs, we propose the *Label MSE* transferability estimators, which replaces $w^*(x_i^t)$ by the "dummy" source label $z_i = h^*(w^*(x_i^t))$. Using dummy labels from the trained source model (w^*, h^*) is a technique previously used to compute the LEEP transferability score for classification tasks (Nguyen et al., 2020). We formally define this family of estimators below.

Definition 2 (Label MSE). *A Label MSE transferability estimator between a source dataset $\mathcal{D}_s$ and a target dataset $\mathcal{D}_t$, with a regularization parameter $\lambda \geq 0$, is defined as: $\mathcal{T}_\lambda^{\text{lab}}(\mathcal{D}_s, \mathcal{D}_t) := \min_{A,B} \left\{ \frac{1}{n_t} \sum_{i=1}^{n_t} \|y_i^t - Az_i - B\|^2 + \lambda \|A\|_F^2 \right\}$, where $A \in \mathbb{R}^{d_s \times d_t}$ is a $d_s \times d_t$ real-valued matrix, $B \in \mathbb{R}^{d_t}$ is a d_t-dimensional real-valued vector, and $z_i = h^*(w^*(x_i^t)), \forall i$.*

From our definitions, note that the lower the Linear MSE or Label MSE, the better the transferability. Since the size of z_i is usually much smaller than that of $w^*(x_i^t)$ (i.e., $d_s \ll d_r$), computing the Label MSE is usually faster than computing the Linear MSE. On the other hand, while the Linear MSE can be interpreted as an approximation to $\mathcal{L}(w^*, k^*; \mathcal{D}_t)$ using a (regularized) linear regression head, properties of the Label MSE is not well understood. In Section 3, we shall prove novel theoretical properties showing the connection between the Label MSE and the expected MSE of the target model (w^*, k^*). In Section 5, we will evaluate the performance of these estimators empirically.

3 Theoretical Properties of Label MSE

In this section, we prove some theoretical properties for the Label MSE with ReLU feed-forward neural networks. These properties are given in the form of the generalization bounds relating the expected risk of the transferred model (w^*, k^*) and the Label MSE. To prove these bounds, we make the standard assumption that the source dataset $\mathcal{D}_s$ and the target dataset $\mathcal{D}_t$ are drawn i.i.d from the unknown distributions $\mathbb{P}(X^s, Y^s)$ and $\mathbb{P}(X^t, Y^t)$ respectively; that is, $(x_i^s, y_i^s) \overset{\text{i.i.d}}{\sim} \mathbb{P}(X^s, Y^s)$ and $(x_i^t, y_i^t) \overset{\text{i.i.d}}{\sim} \mathbb{P}(X^t, Y^t)$. Given any model (w, k) for the target task, the expected risk (or true risk) of (w, k) is defined as:

$$\mathcal{R}(w, k) = \mathbb{E}_{(x^t, y^t) \sim \mathbb{P}(X^t, Y^t)} \left\{ \|y^t - k(w(x^t))\|^2 \right\}. \tag{4}$$

Throughout the section, we will assume the space of all target regression heads k, which may have more than one layer, is a superset of all the linear regression models. This assumption is generally true for ReLU networks (Arora et al., 2018). First, we prove the following lemma relating the empirical MSE loss $\mathcal{L}(w^*, k^*; \mathcal{D}_t)$ of the transferred target model (w^*, k^*) and the Label MSE. This lemma shows the Label MSE upper bounds the transferred target model's empirical loss. The proof for this lemma is in Appendix A.1.

Lemma 1. *Let (w^*, k^*) be the transferred target model obtained from Eq.* (1) *and* (3). *For all $\lambda \geq 0$, we have: $\mathcal{L}(w^*, k^*; \mathcal{D}_t) \leq \mathcal{T}_\lambda^{\text{lab}}(\mathcal{D}_s, \mathcal{D}_t)$.*

To derive the generalization bound for $\mathcal{R}(w^*, k^*)$, we also need to prove the uniform bound in Lemma 2 below. In this lemma, L is the number of layers of the ReLU feed-forward neural network (w, k), and we assume the number of hidden nodes and parameters in each layer are upper bounded by H and $M \geq 1$ respectively. Without loss of generality, we also assume all input and output data are upper bounded by 1 in ℓ_∞-norm. This assumption can easily be satisfied by a pre-processing step that scales them to $[0, 1]$ in ℓ_∞-norm. The proof for this lemma is in Appendix A.2.

Lemma 2. *For any $\delta > 0$, with probability at least $1 - \delta$, for all ReLU feed-forward neural network (w, k) of the target task, we have: $|\mathcal{R}(w, k) - \mathcal{L}(w, k; \mathcal{D}_t)| \leq C(d, d_t, M, H, L, \delta)/\sqrt{n_t}$, where $C(d, d_t, M, H, L, \delta) = 16M^{2L+2}H^{2L}[d_t^2 d\sqrt{L + 1 + \ln d} + d_t d^2 \sqrt{2\ln(4/\delta)}]$.*

Applying Lemma 1 and 2 for (w^*, k^*), we obtain the following generalization bound for $\mathcal{R}(w^*, k^*)$.

Theorem 1. *For any $\lambda \geq 0$ and $\delta > 0$, with probability at least $1 - \delta$, we have:*

$$\mathcal{R}(w^*, k^*) \leq \mathcal{T}_\lambda^{\text{lab}}(\mathcal{D}_s, \mathcal{D}_t) + C(d, d_t, M, H, L, \delta)/\sqrt{n_t}.$$

This theorem shows that the expected risk $\mathcal{R}(w^*, k^*)$ is upper bounded by the Label MSE $\mathcal{T}_\lambda^{\text{lab}}(\mathcal{D}_s, \mathcal{D}_t)$ plus a complexity term $C(d, d_t, M, H, L, \delta)/\sqrt{n_t}$ that depends on the target dataset (specifically, the input and output dimensions, as well as the dataset size) and the architecture of the target network. When the complexity term is small (e.g., when n_t is large enough), the Label MSE will be a tighter bound for the expected risk.

Special Case with Same Input Set. When the source and target datasets have the same input set, i.e., $\mathcal{D}_s = \{(x_i, y_i^s)\}_{i=1}^n$ and $\mathcal{D}_t = \{(x_i, y_i^t)\}_{i=1}^n$, we can compute the Label MSE directly from the labels without training the source model (w^*, h^*) or computing the dummy labels. Particularly, we can consider the following new definition for the Label MSE:

$$\widehat{\mathcal{T}}_\lambda^{\text{lab}}(\mathcal{D}_s, \mathcal{D}_t) := \min_{A,B} \left\{ \frac{1}{n} \sum_{i=1}^n \|y_i^t - Ay_i^s - B\|^2 + \lambda \|A\|_F^2 \right\}. \tag{5}$$

In this new definition, the Label MSE is computed by training a Ridge regression model directly from the corresponding label pairs (y_i^s, y_i^t), which is **less expensive** since we do not need to train the source model. We can also prove similar generalization bounds with $\widehat{\mathcal{T}}_\lambda^{\text{lab}}(\mathcal{D}_s, \mathcal{D}_t)$. In the followings, denote $A_\lambda^*, B_\lambda^* := \operatorname{argmin}_{A,B} \left\{ \frac{1}{n} \sum_{i=1}^n \|y_i^t - Ay_i^s - B\|^2 + \lambda \|A\|_F^2 \right\}$. We first show the following lemma for the empirical loss $\mathcal{L}(w^*, k^*; \mathcal{D}_t)$ of the transferred target model (w^*, k^*).

Lemma 3. *Let w^*, h^*, k^* be the models obtained from Eq.* (1) *and* (3). *For any $\lambda \geq 0$, we have: $\sqrt{\mathcal{L}(w^*, k^*; \mathcal{D}_t)} \leq \sqrt{\widehat{\mathcal{T}}_\lambda^{\text{lab}}(\mathcal{D}_s, \mathcal{D}_t)} + \|A_\lambda^*\|_F \sqrt{\mathcal{L}(w^*, h^*; \mathcal{D}_s)}$.*

The proof for this lemma is in Appendix A.3. Using Lemma 2 and 3, we obtain the following generalization bound for the expected risk $\mathcal{R}(w^*, k^*)$ in this setting with shared inputs.

Theorem 2. *For any $\lambda \geq 0$ and $\delta > 0$, with probability at least $1 - \delta$, we have:*

$$\sqrt{\mathcal{R}(w^*, k^*)} \leq \sqrt{\widehat{\mathcal{T}}_\lambda^{\text{lab}}(\mathcal{D}_s, \mathcal{D}_t)} + \|A_\lambda^*\|_F \sqrt{\mathcal{L}(w^*, h^*; \mathcal{D}_s)} + \sqrt{C(d, d_t, M, H, L, \delta)}/n^{\frac{1}{4}}.$$

The proof for this theorem is in Appendix A.4. From the theorem, the Label MSE $\widehat{\mathcal{T}}_\lambda^{\text{lab}}(\mathcal{D}_s, \mathcal{D}_t)$ can indirectly tell us information about the expected risk $\mathcal{R}(w^*, k^*)$ without actually training w^*, h^*, and k^*. This bound becomes tighter when n is large or $\mathcal{L}(w^*, h^*; \mathcal{D}_s)$ is small (e.g., when the source model is expressive enough to fit the source data). An experiment to investigate the usefulness of our bounds is given in Appendix B.3.

4 Related Work

Our paper is one of the recent attempts to develop transferability estimators for deep transfer learning (Bao et al., 2019; Tran et al., 2019; Nguyen et al., 2020; Deshpande et al., 2021; Li et al., 2021; Tan et al., 2021; You et al., 2021; Huang et al., 2022) that can effectively predict the effectiveness of transfer learning between two given tasks with little computation. Most of the existing work for transferability estimation focuses on classification (Bao et al., 2019; Tran et al., 2019; Nguyen et al., 2020; Deshpande et al., 2021; Li et al., 2021; Tan et al., 2021), while there are only two methods developed for regression (You et al., 2021; Huang et al., 2022). One method, called LogME (You et al., 2021), takes a Bayesian approach and uses the maximum log evidence of the target data as the transferability estimator. While this method can be sped up using matrix decomposition, its scalability is still limited since the required memory is large. In contrast, our approaches here are simpler, faster, and more effective. Furthermore, we provide novel theoretical properties for our methods that were not available for LogME. Another approach for transferability estimation between regression tasks, proposed by Huang et al. (2022), is to divide the real-valued outputs into different bins and apply a classification transferability estimator. In our experiments, we show that this approach is less accurate than both LogME and our approaches.

Transferability can also be inferred from a task taxonomy (Zamir et al., 2018; Dwivedi & Roig, 2019; Dwivedi et al., 2020) or a task space representation (Achille et al., 2019), which embeds tasks as vectors on a vector space. A popular task taxonomy, Taskonomy (Zamir et al., 2018), exploits the underlying structure of visual tasks by computing a task affinity matrix that can be used for estimating transferability. Constructing the Taskonomy requires training of a small classification head, which resembles the training of the (regularized) linear regression models in our approaches. However, they investigate the global taxonomy of classification tasks, while our paper studies regression tasks with a focus on estimating their transferability efficiently.

Our paper is also related to transfer learning for deep models (Tan et al., 2018), which has been successfully used in real-world regression problems such as music tagging (Choi et al., 2017; Manco et al., 2022), object detection and localization (Cai et al., 2020; Bu et al., 2021), landmark detection (Fard et al., 2021; Poster et al., 2021), or pose estimation (Schwarz et al., 2015; Doersch & Zisserman, 2019). Several previous works have investigated theoretical bounds for transfer learning (Ben-David & Schuller, 2003; Blitzer et al., 2007; Mansour et al., 2009; Azizzadenesheli et al., 2019; Wang et al., 2019; Tripuraneni et al., 2020); however, these bounds are hard to compute in practice and thus unsuitable for transferability estimation. Some previous transferability estimators have theoretical bounds on the empirical loss (Tran et al., 2019; Nguyen et al., 2020), but they were shown for classification and did not bound the expected loss. Our work, on the other hand, focuses on regression and proves generalization bounds for the expected loss.

5 Experiments

In this section, we conduct experiments to evaluate our transferability estimators on the keypoint (or landmark) regression tasks using the following two large-scale public datasets:

• **CUB-200-2011** (Wah et al., 2011). This dataset contains 11,788 bird images with 15 labeled keypoints indicating 15 different parts of a bird body. We use 9,788 images for training and 2,000 images for testing. Since the annotations for occluded keypoints are highly inaccurate, we remove all occluded keypoints during the training for both source and target tasks.

• **OpenMonkey** (Yao et al., 2021). This is a benchmark for non-human pose tracking problems. It offers over 100,000 monkey images in natural contexts, annotated with 17 body landmarks. We use the original train-test split, which contains 66,917 images for training and 22,306 images for testing.

In our experiments, we use ResNet34 (He et al., 2016) as the model backbone since it provides good performance as a source model. Following previous work (Tran et al., 2019; Nguyen et al.,

Table 1: **Correlation coefficients when transferring from OpenMonkey to CUB-200-2011** for different transferability estimators. Bold numbers indicate the best results in each row. Asterisks (*) indicate the best results among the corresponding label-based or feature-based methods. Detailed correlation plots are in Figure 5- 7 in the Appendix.

Transfer setting	Label-based method				Feature-based method			
	LabLogME (2021)	LabTransRate (2022)	LabMSE0 (ours)	LabMSE1 (ours)	LogME (2021)	TransRate (2022)	LinMSE0 (ours)	LinMSE1 (ours)
Head re-training	0.958	0.165	**0.992***	**0.992***	0.969	0.121	0.982	0.988*
Half fine-tuning	0.706	0.392	**0.882***	**0.882***	0.870	0.304	0.865	0.872*
Full fine-tuning	0.691	0.410	**0.870***	**0.870***	0.861*	0.311	0.854	0.861*

2020), we investigate how well our transferability estimators correlate (using Pearson correlation) with the *test* MSE of the target model obtained from actual transfer learning. We consider three transfer learning algorithms: (1) **head re-training**: We fix all layers of the source model up until the penultimate layer and re-train the last fully-connected (FC) layer using the target training set; (2) **half fine-tuning**: We fine-tune the last convolutional block and all the FC layers of the source model, while keeping all other layers fixed; and (3) **full fine-tuning**: We fine-tune the whole source model using the target training set. Among these settings, head re-training resembles the transfer scenario in Section 2.1, while half fine-tuning and full fine-tuning are more commonly used in practice. For half fine-tuning, around half of the parameters in the network will be fine-tuned ($\sim$13M parameters). More details of our experiment settings are in Appendix B.1.

We shall compare our transferability estimators, Linear MSE and Label MSE, with two recent SotA baselines for regression: LogME (You et al., 2021) and TransRate (Huang et al., 2022). For our methods, we consider $\lambda = 0$ (named **LinMSE0** and **LabMSE0**) for the estimators without regularization, and $\lambda = 1$ (named **LinMSE1** and **LabMSE1**) for the estimators with the default λ setting. The effects of λ on our algorithms are investigated in Appendix B.2. For LogME and TransRate baselines, besides the usual versions (named **LogME** and **TransRate**) that are computed from the extracted features and the target labels, we also consider the versions where they are computed from the dummy labels and the target labels (named **LabLogME** and **LabTransRate**). As in Huang et al. (2022), we divide the target label values into equal-sized bins (five bins in our case) to compute TransRate and LabTransRate.

5.1 General Transfer Between Two Different Domains

This experiment considers the general case where source models are trained on one dataset (OpenMonkey) and then transferred to another (CUB-200-2011). Specifically, we train a source model for each of the 17 keypoints of the OpenMonkey dataset and transfer them to each of the 15 keypoints of the CUB-200-2011 dataset, resulting in a total of 255 final models. Since each keypoint consists of x and y positions, all source and target tasks in this experiment have two dimensional labels. The actual MSEs of these models are computed on the respective test sets and then used to calculate the Pearson correlation coefficients with the transferability estimators. In this experiment, LabMSE0, LabMSE1, LabLogME, and LabTransRate are computed from the dummy labels and the actual target labels.

Results for this experiment are shown in Table 1, with detailed correlation plots given in Figure 5- 7 in the Appendix. From the results, TransRate and LabTransRate perform poorly in this regression setting, while our methods are equal or better than LogME and LabLogME in all cases, especially when using $\lambda = 1$ (LinMSE1) or dummy labels (LabMSE0 and LabMSE1). We also observe that adding a regularizer in LabMSE1 does not significantly change its correlation coefficient compared to LabMSE0. This is because the labels are already scaled to $[0, 1]$, so a regularizer with $\lambda = 1$ has negligible effect on the scores (see Appendix B.2 for more experiments on the effects of λ). We will observe the same effect in subsequent experiments. It is also surprising that LabMSE0 and LabMSE1 are better than LinMSE0 and LinMSE1. One possible explanation for this phenomenon is that the dummy labels (i.e., body parts of monkeys) give more information about the target labels (i.e., body parts of birds) than the extracted features.

Table 2: **Correlation coefficients when transferring between tasks with shared inputs** for different transferability estimators. Bold numbers indicate the best results in each row. Asterisks (*) indicate the best results among the corresponding label-based or feature-based methods. Detailed correlation plots are in Figure 8-13 in the Appendix.

Dataset	Transfer setting	Label-based method				Feature-based method			
		LabLogME (2021)	LabTransRate (2022)	LabMSE0 (ours)	LabMSE1 (ours)	LogME (2021)	TransRate (2022)	LinMSE0 (ours)	LinMSE1 (ours)
CUB-200-2011	Head re-training	0.547	0.008	0.916*	0.916*	0.889	0.029	0.921	**0.932***
	Half fine-tuning	0.400	0.006	0.536*	0.536*	0.560	0.006	**0.628***	0.607
	Full fine-tuning	**0.120***	0.001	0.056	0.056	0.099	0.100*	0.097	0.093
OpenMonkey	Head re-training	0.890	0.666	0.973*	0.973*	0.646	0.711	0.949	**0.981***
	Half fine-tuning	0.615	0.340	0.754*	0.754*	0.391	0.488	**0.893***	0.787
	Full fine-tuning	0.569	0.269	0.705*	0.705*	0.352	0.439	**0.852***	0.739

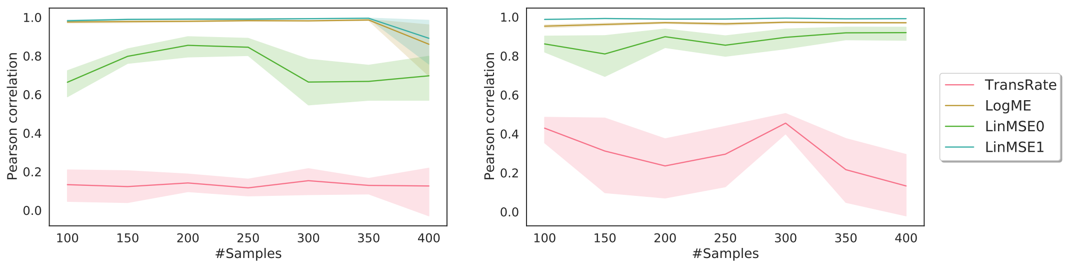

Figure 1: **Correlation coefficients with respect to different target training set sizes** for 4 transferability estimators on CUB-200-2011 (left) and OpenMonkey (right).

5.2 Transfer Between Tasks with Shared Input Set

In this experiment, we consider the setting where the source and target tasks have the same inputs. Since images in our datasets contain multiple labels (15 keypoints for CUB-200-2011 and 17 keypoints for OpenMonkey), we can use any two different keypoints on the same dataset as source and target tasks. In total, we can construct 210 source-target pairs for CUB-200-2011 and 272 pairs for OpenMonkey that all have the same source and target inputs but different labels. The labels for all source and target tasks are also two dimensional real values. We repeat the experiment in Section 5.1 with these source-target pairs for CUB-200-2011 and OpenMonkey separately. The main difference in this experiment is that we use the *true* source labels (instead of dummy labels) when computing LabLogME, LabTransRate, LabMSE0, and LabMSE1. Thus, these estimators can be computed without any source models (and hence, incurring very low computational costs) in this setting.

Results for these experiments are given in Table 2, with detailed correlation plots in Figure 8-13 in the Appendix. In the results, both versions of TransRate perform poorly on CUB-200-2011, while TransRate is slightly better than LogME on OpenMonkey. In 5/6 settings in Table 2 (i.e., head re-training and half fine-tuning on CUB-200-2011, as well as all three settings for OpenMonkey), LabMSE0 and LabMSE1 both outperform LabLogME and LabTransRate, while LinMSE0 and LinMSE1 also outperform LogME and TransRate. In these five settings, the LinMSE methods achieve the best correlations overall. In the remaining setting where we transfer by full fine-tuning on the CUB-200-2011 dataset, all methods perform poorly.

We also report in Table 5 and 6 (see the Appendix) more comprehensive results for all source tasks on CUB-200-2011 and OpenMonkey respectively. Each row of the tables corresponds to one source task and shows the correlation coefficients when transferring to all other tasks in the respective dataset. From the tables, our transferability estimators are consistently better than LogME, LabLogME, TransRate, and LabTransRate for most source tasks on both datasets. These results further confirm the effectiveness of our proposed methods.

5.3 Evaluations on Small Target Sets

In many real-world transfer learning scenarios, the target set is usually small. This experiment will evaluate the effectiveness of the feature-based transferability estimators (LogME, TransRate, LinMSE0, and LinMSE1) in this small data regime where the number of samples is smaller than the

Table 3: **Average running time** (in milliseconds) of different transferability estimators. The bold number indicates the best result. Asterisks (*) indicate the best results among the corresponding label-based or feature-based methods.

Label-based method				Feature-based method			
LabLogME (2021)	LabTransRate (2022)	LabMSE0 (ours)	LabMSE1 (ours)	LogME (2021)	TransRate (2022)	LinMSE0 (ours)	LinMSE1 (ours)
3.55 ± 0.04	4.11 ± 0.18	2.87 ± 0.15	$\mathbf{2.58} \pm \mathbf{0.14}$*	112.99 ± 1.18	94.57 ± 0.91	107.48 ± 3.60	27.41 ± 0.89*

feature dimension. For this experiment, we fix a source task (*Belly* for CUB-200-2011 and *Right eye* for OpenMonkey) and transfer to all other tasks in the corresponding dataset using head re-training. For each target task, instead of using the full data, we randomly select a subset of 100 to 400 images to perform transfer learning and to compute the transferability scores. The actual MSEs of the transferred models are still computed using the full target test sets.

Figure 1 compares the correlations of the 4 methods on different target set sizes between 100 and 400. The results are averaged over 10 runs with 10 different random seeds. From the figure, LogME and LinMSE1 are better than TransRate and LinMSE0. This is expected since LogME and LinMSE1 are designed to avoid overfitting on small data. Both LogME and LinMSE1 are also more stable, but LinMSE1 is slightly better than LogME on all dataset sizes.

5.4 Efficiency of Our Methods

One of the main strengths of our methods is their efficiency, due to the simplicity of training the Ridge regression head. In this experiment, we first use the settings in Section 5.2 to compare the running time of our methods with that of the baselines on the CUB-200-2011 dataset. Table 3 reports the results (averaged over 5 runs with different random seeds) for this experiment.

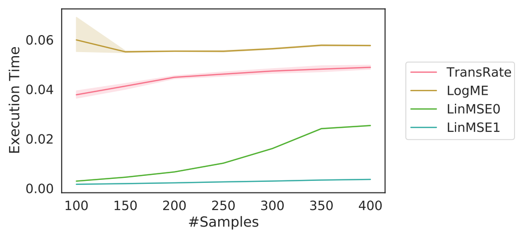

Figure 2: **Average running time** (milliseconds) with respect to different target training set sizes.

From these results, our proposed methods, LabMSE0, LabMSE1, LinMSE0, and LinMSE1, are all faster than the corresponding label-based or feature-based baselines. The table also shows that LabMSE1 and LinMSE1 achieve the best running time among the label-based and feature-based methods respectively.

In Figure 2, we also compare the average running time of the 4 transferability estimators using the CUB-200-2011 experiment in Section 5.3. This figure clearly shows that our methods, LinMSE0 and LinMSE1, are more computationally efficient than LogME and TransRate. Both results in Table 3 and Figure 2 show that LinMSE1 and LabMSE1 are significantly faster than other feature-based and label-based methods respectively. In these experiments, LinMSE1 and LabMSE1 converge faster than LinMSE0 and LabMSE0 respectively, and thus are more efficient.

5.5 Source Task Selection

Source task selection is important for applying transfer learning. It allows us to choose the right source data or model that can offer the best transfer learning performance. In this experiment, we examine the application of our transferability estimation methods for selecting source data on the CUB-200-2011 dataset. We use the head re-training setting similar to Section 5.2, but fix one of the tasks as the target and choose the best source task from the rest of the task pool. We repeat this process for all 15 target tasks and measure the top-k matching rate of each transferability measure. The top-k matching rate is defined as $m_{\text{match}}/m_{\text{target}}$, where m_{target} is the total number of target tasks (15 in our case), and m_{match} is the number of times the selected source task gives a target model within the best k models. Here the best k models are determined by the actual test MSE on the target task.

According to our experiment results, the *top-*5 *matching rates* obtained are: 0/15 (LabLogME), 0/15 (LabTransRate), 15/15 (LabMSE0), 15/15 (LabMSE1), 15/15 (LogME), 0/15 (TransRate), 15/15 (LinMSE0), and 15/15 (LinMSE1), while the *top-*3 *matching rates* are: 0/15 (LabLogME), 0/15 (LabTransRate), 0/15 (LabMSE0), 0/15 (LabMSE1), 15/15 (LogME), 0/15 (TransRate), 15/15 (LinMSE0), and 15/15 (LinMSE1). We also observe that all transferability scores perform equally poorly

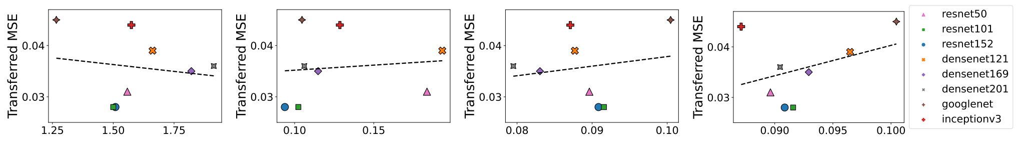

(a) LogME (2021) (b) TransRate (2022) (c) LinMSE0 (ours) (d) LinMSE1 (ours)

Figure 3: **Actual transferred MSEs vs. transferability scores** when transferring from pre-trained classification models to a target regression task. A linear regression model (dashed line) is fitted to the points in each plot.

(0/15) on top-1 metric. These results show our methods, LinMSE0 and LinMSE1, are comparable with LogME for source task selection. When the source models are not available (i.e., LogME, TransRate, LinMSE0, and LinMSE1 are not readily available), our methods (LabMSE0 and LabMSE1) are better than LabLogME for source dataset selection, measured by the top-5 metric.

5.6 Beyond Regression

Although our paper mainly focuses on regression tasks, the main idea of using the penalized MSE of a Ridge regression model for transferability estimation goes beyond regression. In principle, this idea can be applied for transferring between classification tasks (in this case, we should train a linear classifier and use its penalized accuracy as the transferability estimator) or between a classification and a regression task.

In this section, we describe an experiment where we transfer from a classification task to a regression task. Particularly, we use 8 source models pre-trained on ImageNet (Deng et al., 2009) and transfer to a target regression task on the *dSprite* dataset (Matthey et al., 2017) using full fine-tuning. The settings for this experiment are similar to that of You et al. (2021) where the target task is a regression task with 4-dimensional labels: x and y positions, scale, and orientation. We compute the transferability scores from the extracted features and the labels of the target training set. More details about the settings for this experiment are in Appendix B.1.

Figure 3 shows the results for this experiment. From the figure, the prediction trends for LogME, LinMSE0, and LinMSE1 are correct, while that of TransRate is not correct. To compare these methods, we fit a linear regression model to the points in each plot and compute its RMSE to these points. The RMSEs for each plot are: 6.12×10^{-3} (LogME), 6.16×10^{-3} (TransRate), 6.10×10^{-3} (LinMSE0), and 5.73×10^{-3} (LinMSE1). These results show that our methods, LinMSE0 and LinMSE1, are better than the LogME and TransRate baselines in this setting.

5.7 Additional Experiments

Effects of λ. In Appendix B.2 and Table 4, we describe an additional experiment to investigate the effects of λ on the performance of our methods. The results show that our methods are generally robust to the value of λ and give better correlations than the baselines for a wide range of λ values.

Usefulness of Theoretical Bounds. In Appendix B.3, we conduct an experiment to investigate the usefulness of our theory in Section 3. This experiment indicates that the complexity term in our bounds may have little effects for transferability estimation, as opposed to the transferability score term that has a strong effect.

Tasks with Higher Dimensional Labels. In Appendix B.4, we describe an additional experiment where the output tasks have higher dimensional labels (10 dimensions). The experiment also shows our methods are better than the baselines in this case.

6 Conclusion

We explored Linear MSE and Label MSE, two families of simple but effective transferability estimation methods for regression tasks. We proved novel theoretical bounds for the expected risk of the target models using these estimators, both for the general setting and the shared inputs setting. Our extensive experiments showed that our methods are superior to recent, relevant SotA methods in terms of efficiency and effectiveness. Our proposed ideas can also be extended to mixed cases where one of the two tasks is a classification problem.

REFERENCES

Alessandro Achille, Michael Lam, Rahul Tewari, Avinash Ravichandran, Subhransu Maji, Charless C Fowlkes, Stefano Soatto, and Pietro Perona. Task2vec: Task embedding for meta-learning. In *IEEE/CVF Conference on Computer Vision and Pattern Recognition*, pp. 6430–6439, 2019.

Pulkit Agrawal, Ross Girshick, and Jitendra Malik. Analyzing the performance of multilayer neural networks for object recognition. In *European Conference on Computer Vision*, 2014.

Raman Arora, Amitabh Basu, Poorya Mianjy, and Anirbit Mukherjee. Understanding deep neural networks with rectified linear units. In *International Conference on Learning Representations*, 2018.

Kamyar Azizzadenesheli, Anqi Liu, Fanny Yang, and Animashree Anandkumar. Regularized learning for domain adaptation under label shifts. In *International Conference on Learning Representations*, 2019.

Yajie Bao, Yang Li, Shao-Lun Huang, Lin Zhang, Lizhong Zheng, Amir Zamir, and Leonidas Guibas. An information-theoretic approach to transferability in task transfer learning. In *IEEE International Conference on Image Processing*, 2019.

Shai Ben-David and Reba Schuller. Exploiting task relatedness for multiple task learning. *Learning theory and kernel machines*, pp. 567–580, 2003.

John Blitzer, Koby Crammer, Alex Kulesza, Fernando Pereira, and Jennifer Wortman. Learning bounds for domain adaptation. In *Advances in Neural Information Processing Systems*, 2007.

Daniel Bolya, Rohit Mittapalli, and Judy Hoffman. Scalable diverse model selection for accessible transfer learning. In *Advances in Neural Information Processing Systems*, 2021.

Xingyuan Bu, Junran Peng, Junjie Yan, Tieniu Tan, and Zhaoxiang Zhang. GAIA: A transfer learning system of object detection that fits your needs. In *IEEE/CVF Conference on Computer Vision and Pattern Recognition*, pp. 274–283, 2021.

Enyu Cai, Sriram Baireddy, Changye Yang, Melba Crawford, and Edward J Delp. Deep transfer learning for plant center localization. In *IEEE/CVF Conference on Computer Vision and Pattern Recognition Workshops*, pp. 62–63, 2020.

Ken Chatfield, Karen Simonyan, Andrea Vedaldi, and Andrew Zisserman. Return of the devil in the details: Delving deep into convolutional nets. In *British Machine Vision Conference*, 2014.

Keunwoo Choi, György Fazekas, Mark Sandler, and Kyunghyun Cho. Transfer learning for music classification and regression tasks. In *International Society for Music Information Retrieval Conference*, pp. 141–149, 2017.

Jia Deng, Wei Dong, Richard Socher, Li-Jia Li, Kai Li, and Li Fei-Fei. ImageNet: A large-scale hierarchical image database. In *IEEE/CVF Conference on Computer Vision and Pattern Recognition*, 2009.

Aditya Deshpande, Alessandro Achille, Avinash Ravichandran, Hao Li, Luca Zancato, Charless Fowlkes, Rahul Bhotika, Stefano Soatto, and Pietro Perona. A linearized framework and a new benchmark for model selection for fine-tuning. *arXiv preprint arXiv:2102.00084*, 2021.

Guneet S. Dhillon, Pratik Chaudhari, Avinash Ravichandran, and Stefano Soatto. A baseline for few-shot image classification. In *International Conference on Learning Representations*, 2020.

Carl Doersch and Andrew Zisserman. Sim2real transfer learning for 3D human pose estimation: motion to the rescue. In *Advances in Neural Information Processing Systems*, 2019.

Jeff Donahue, Yangqing Jia, Oriol Vinyals, Judy Hoffman, Ning Zhang, Eric Tzeng, and Trevor Darrell. Decaf: A deep convolutional activation feature for generic visual recognition. In *International Conference on Machine Learning*, pp. 647–655, 2014.

Kshitij Dwivedi and Gemma Roig. Representation similarity analysis for efficient task taxonomy & transfer learning. In *IEEE/CVF Conference on Computer Vision and Pattern Recognition*, pp. 12387–12396, 2019.

Kshitij Dwivedi, Jiahui Huang, Radoslaw Martin Cichy, and Gemma Roig. Duality diagram similarity: a generic framework for initialization selection in task transfer learning. In *European Conference on Computer Vision*, pp. 497–513, 2020.

Ali Pourramezan Fard, Hojjat Abdollahi, and Mohammad Mahoor. ASMNet: A lightweight deep neural network for face alignment and pose estimation. In *IEEE/CVF Conference on Computer Vision and Pattern Recognition Workshops*, pp. 1521–1530, 2021.

Ross Girshick, Jeff Donahue, Trevor Darrell, and Jitendra Malik. Rich feature hierarchies for accurate object detection and semantic segmentation. In *IEEE/CVF Conference on Computer Vision and Pattern Recognition*, 2014.

Noah Golowich, Alexander Rakhlin, and Ohad Shamir. Size-independent sample complexity of neural networks. In *Annual Conference on Learning Theory*, 2018.

Kaiming He, Xiangyu Zhang, Shaoqing Ren, and Jian Sun. Deep residual learning for image recognition. In *IEEE/CVF Conference on Computer Vision and Pattern Recognition*, 2016.

Gao Huang, Zhuang Liu, Laurens Van Der Maaten, and Kilian Q Weinberger. Densely connected convolutional networks. In *IEEE/CVF Conference on Computer Vision and Pattern Recognition*, 2017.

Jiaji Huang, Qiang Qiu, and Kenneth Church. Exploiting a zoo of checkpoints for unseen tasks. In *Advances in Neural Information Processing Systems*, 2021.

Long-Kai Huang, Junzhou Huang, Yu Rong, Qiang Yang, and Ying Wei. Frustratingly easy transferability estimation. In *International Conference on Machine Learning*, 2022.

Yandong Li, Xuhui Jia, Ruoxin Sang, Yukun Zhu, Bradley Green, Liqiang Wang, and Boqing Gong. Ranking neural checkpoints. In *IEEE/CVF Conference on Computer Vision and Pattern Recognition*, 2021.

Ilya Loshchilov and Frank Hutter. Decoupled weight decay regularization. In *International Conference on Learning Representations*, 2019.

Ilaria Manco, Emmanouil Benetos, Elio Quinton, and György Fazekas. Learning music audio representations via weak language supervision. In *IEEE International Conference on Acoustics, Speech and Signal Processing*, pp. 456–460, 2022.

Yishay Mansour, Mehryar Mohri, and Afshin Rostamizadeh. Domain adaptation: Learning bounds and algorithms. In *Annual Conference on Learning Theory*, 2009.

Loic Matthey, Irina Higgins, Demis Hassabis, and Alexander Lerchner. dSprites: Disentanglement testing Sprites dataset, 2017. `https://github.com/deepmind/dsprites-dataset/`.

Cuong V Nguyen, Tal Hassner, Matthias Seeger, and Cedric Archambeau. LEEP: A new measure to evaluate transferability of learned representations. In *International Conference on Machine Learning*, 2020.

Maxime Oquab, Leon Bottou, Ivan Laptev, and Josef Sivic. Learning and transferring mid-level image representations using convolutional neural networks. In *IEEE/CVF Conference on Computer Vision and Pattern Recognition*, 2014.

Adam Paszke, Sam Gross, Francisco Massa, Adam Lerer, James Bradbury, Gregory Chanan, Trevor Killeen, Zeming Lin, Natalia Gimelshein, Luca Antiga, et al. Pytorch: An imperative style, high-performance deep learning library. In *Advances in Neural Information Processing Systems*, 2019.

Domenick D Poster, Shuowen Hu, Nathan J Short, Benjamin S Riggan, and Nasser M Nasrabadi. Visible-to-thermal transfer learning for facial landmark detection. *IEEE Access*, 9:52759–52772, 2021.

Max Schwarz, Hannes Schulz, and Sven Behnke. RGB-D object recognition and pose estimation based on pre-trained convolutional neural network features. In *IEEE International Conference on Robotics and Automation*, pp. 1329–1335, 2015.

Shai Shalev-Shwartz and Shai Ben-David. *Understanding machine learning: From theory to algorithms*. Cambridge University Press, 2014.

Ali Sharif Razavian, Hossein Azizpour, Josephine Sullivan, and Stefan Carlsson. CNN features off-the-shelf: An astounding baseline for recognition. In *IEEE/CVF Conference on Computer Vision and Pattern Recognition Workshops*, 2014.

Christian Szegedy, Wei Liu, Yangqing Jia, Pierre Sermanet, Scott Reed, Dragomir Anguelov, Dumitru Erhan, Vincent Vanhoucke, and Andrew Rabinovich. Going deeper with convolutions. In *IEEE/CVF Conference on Computer Vision and Pattern Recognition*, 2015.

Christian Szegedy, Vincent Vanhoucke, Sergey Ioffe, Jon Shlens, and Zbigniew Wojna. Rethinking the inception architecture for computer vision. In *IEEE/CVF Conference on Computer Vision and Pattern Recognition*, 2016.

Chuanqi Tan, Fuchun Sun, Tao Kong, Wenchang Zhang, Chao Yang, and Chunfang Liu. A survey on deep transfer learning. In *International Conference on Artificial Neural Networks*, 2018.

Yang Tan, Yang Li, and Shao-Lun Huang. OTCE: A transferability metric for cross-domain cross-task representations. In *IEEE/CVF Conference on Computer Vision and Pattern Recognition*, 2021.

Xinyi Tong, Xiangxiang Xu, Shao-Lun Huang, and Lizhong Zheng. A mathematical framework for quantifying transferability in multi-source transfer learning. In *Advances in Neural Information Processing Systems*, 2021.

Anh T Tran, Cuong V Nguyen, and Tal Hassner. Transferability and hardness of supervised classification tasks. In *IEEE/CVF International Conference on Computer Vision*, 2019.

Nilesh Tripuraneni, Michael Jordan, and Chi Jin. On the theory of transfer learning: The importance of task diversity. In *Advances in Neural Information Processing Systems*, pp. 7852–7862, 2020.

Catherine Wah, Steve Branson, Peter Welinder, Pietro Perona, and Serge Belongie. The Caltech-UCSD Birds-200-2011 Dataset. *Technical Report*, 2011. `https://authors.library.caltech.edu/27452/`.

Boyu Wang, Jorge Mendez, Mingbo Cai, and Eric Eaton. Transfer learning via minimizing the performance gap between domains. In *Advances in Neural Information Processing Systems*, 2019.

Paul N Whatmough, Chuteng Zhou, Patrick Hansen, Shreyas Kolala Venkataramanaiah, Jae-sun Seo, and Matthew Mattina. FixyNN: Efficient hardware for mobile computer vision via transfer learning. In *Conference on Systems and Machine Learning*, 2019.

Yuan Yao, Abhiraj Abhiraj Mohan, Eliza Bliss-Moreau, Kristine Coleman, Sienna M Freeman, Christopher J Machado, Jessica Raper, Jan Zimmermann, Benjamin Y Hayden, and Hyun Soo Park. OpenMonkeyChallenge: Dataset and Benchmark Challenges for Pose Tracking of Non-human Primates. *bioRxiv*, 2021. `http://openmonkeychallenge.com/`.

Kaichao You, Yong Liu, Jianmin Wang, and Mingsheng Long. LogME: Practical assessment of pre-trained models for transfer learning. In *International Conference on Machine Learning*, 2021.

Amir R. Zamir, Alexander Sax, William B. Shen, Leonidas J. Guibas, Jitendra Malik, and Silvio Savarese. Taskonomy: Disentangling task transfer learning. In *IEEE/CVF Conference on Computer Vision and Pattern Recognition*. IEEE, 2018.

A Technical Proofs

A.1 Proof of Lemma 1

Denote $A^*, B^* = \operatorname*{argmin}_{A,B} \left\{ \frac{1}{n_t} \sum_{i=1}^{n_t} \|y_i^t - Az_i - B\|^2 + \lambda \|A\|_F^2 \right\}$.

For all k, we have:

$$\begin{aligned}
\sqrt{\mathcal{L}(w^*, k^*; \mathcal{D}_t)} &\leq \sqrt{\mathcal{L}(w^*, k; \mathcal{D}_t)} && \text{(definition of } k^*\text{)} \\
&= \left[\frac{1}{n_t} \sum_{i=1}^{n_t} \|y_i^t - k(w^*(x_i^t))\|^2 \right]^{1/2} && \text{(definition of } \mathcal{L}\text{)} \\
&\leq \left[\frac{1}{n_t} \sum_{i=1}^{n_t} \|y_i^t - A^* z_i - B^*\|^2 \right]^{1/2} + \left[\frac{1}{n_t} \sum_{i=1}^{n_t} \|A^* z_i + B^* - k(w^*(x_i^t))\|^2 \right]^{1/2} \\
& && \text{(triangle inequality)} \\
&\leq \sqrt{\mathcal{T}_\lambda^{\text{lab}}(\mathcal{D}_s, \mathcal{D}_t)} + \left[\frac{1}{n_t} \sum_{i=1}^{n_t} \|A^* z_i + B^* - k(w^*(x_i^t))\|^2 \right]^{1/2} \\
&= \sqrt{\mathcal{T}_\lambda^{\text{lab}}(\mathcal{D}_s, \mathcal{D}_t)} + \left[\frac{1}{n_t} \sum_{i=1}^{n_t} \|A^* h^*(w^*(x_i^t)) + B^* - k(w^*(x_i^t))\|^2 \right]^{1/2}. \\
& && \text{(definition of } z_i\text{)}
\end{aligned}$$

By choosing $k(\cdot) = A^* h^*(\cdot) + B^*$, the second term in the above inequality becomes 0. This implies $\sqrt{\mathcal{L}(w^*, k^*; \mathcal{D}_t)} \leq \sqrt{\mathcal{T}_\lambda^{\text{lab}}(\mathcal{D}_s, \mathcal{D}_t)}$, and thus the lemma holds.

A.2 Proof of Lemma 2

We recall the definition of Rademacher complexity. Given a real-valued function class $\mathcal{G}$ and a set of data points $\mathcal{D} = \{u_i\}_{i=1}^n$, the (empirical) Rademacher complexity $\widehat{R}_\mathcal{D}(\mathcal{G})$ is defined as:

$$\widehat{R}_\mathcal{D}(\mathcal{G}) = \mathbb{E}_\epsilon \left[\sup_{g \in \mathcal{G}} \frac{1}{n} \sum_{i=1}^n \epsilon_i g(u_i) \right],$$

where $\epsilon = (\epsilon_1, \epsilon_2, \ldots, \epsilon_n)$ is a vector uniformly distributed in $\{-1, +1\}^n$.

In our setting, the hypothesis space Φ is the class of L-layer ReLU feed-forward neural networks whose number of hidden nodes and parameters in each layer are bounded from above by H and $M \geq 1$ respectively. For all $(w, k) \in \Phi$ and x such that $\|x\|_\infty \leq 1$, we have:

$$\|k(w(x))\|_\infty \leq d M^{L+1} H^L.$$

Define $f_{w,k}(x, y) = y - k(w(x))$ and note that $f_{w,k}(x, y) \in \mathbb{R}^{d_t}$. For any $j = 1, 2, \ldots, d_t$, let $[\cdot]_j$ be the projection map to the j-th coordinate. We consider the following real-valued function classes:

$$\begin{aligned}
\mathcal{F} &= \{\|f_{w,k}\|^2 : (w, k) \in \Phi\}, \\
\mathcal{F}_j &= \{[f_{w,k}]_j : (w, k) \in \Phi\}, \\
\Phi_j &= \{[k(w(\cdot))]_j : (w, k) \in \Phi\},
\end{aligned}$$

where each element of $\mathcal{F}$ or $\mathcal{F}_j$ is a function with variables (x, y), and each element of Φ_j is a function with variable x. Let $\mathcal{D}_t^x = \{x_i^t\}_{i=1}^{n_t}$ be the set of target inputs. By Theorem 2 of Golowich et al. (2018), for all $j = 1, 2, \ldots, d_t$, we have:

$$\widehat{R}_{\mathcal{D}_t^x}(\Phi_j) \leq 2 d_t M^{L+1} H^L \sqrt{\frac{L + 1 + \ln d}{n_t}}.$$

We note that for any $i = 1, 2, \ldots, n_t$, the function $r_i(a) = (a - y_i^t)^2$ mapping from $a \in [-dM^{L+1}H^L, dM^{L+1}H^L]$ to $\mathbb{R}$ is Lipschitz with constant $4dM^{L+1}H^L$. Thus, applying the Contraction Lemma (Lemma 26.9 in Shalev-Shwartz & Ben-David (2014)), we obtain:

$$\widehat{R}_{\mathcal{D}_t}(\mathcal{F}_j) \le 4dM^{L+1}H^L \widehat{R}_{\mathcal{D}_t^x}(\Phi_j) \le 8dd_tM^{2L+2}H^{2L}\sqrt{\frac{L+1+\ln d}{n_t}}.$$

Therefore, $\widehat{R}_{\mathcal{D}_t}(\mathcal{F}) \le \sum_{j=1}^{d_t} \widehat{R}_{\mathcal{D}_t}(\mathcal{F}_j) \le 8dd_t^2M^{2L+2}H^{2L}\sqrt{\frac{L+1+\ln d}{n_t}}$.

Using this inequality, the result of Lemma 2 follows from Theorem 26.5 in Shalev-Shwartz & Ben-David (2014).

A.3 Proof of Lemma 3

Note that: $A_\lambda^*, B_\lambda^* = \underset{A,B}{\operatorname{argmin}} \left\{ \frac{1}{n} \sum_{i=1}^{n} \|y_i^t - Ay_i^s - B\|^2 + \lambda \|A\|_F^2 \right\}$.

For all k, we have:

$$\begin{aligned}
\sqrt{\mathcal{L}(w^*, k^*; \mathcal{D}_t)} &\le \sqrt{\mathcal{L}(w^*, k; \mathcal{D}_t)} && \text{(definition of } k^*) \\
&= \left[\frac{1}{n} \sum_{i=1}^{n} \|y_i^t - k(w^*(x_i))\|^2 \right]^{1/2} && \text{(definition of } \mathcal{L}) \\
&\le \left[\frac{1}{n} \sum_{i=1}^{n} \|y_i^t - A_\lambda^* y_i^s - B_\lambda^*\|^2 \right]^{1/2} + \left[\frac{1}{n} \sum_{i=1}^{n} \|A_\lambda^* y_i^s + B_\lambda^* - k(w^*(x_i))\|^2 \right]^{1/2} \\
& && \text{(triangle inequality)} \\
&\le \sqrt{\widehat{\mathcal{T}}_\lambda^{\text{lab}}(\mathcal{D}_s, \mathcal{D}_t)} + \left[\frac{1}{n} \sum_{i=1}^{n} \|A_\lambda^* y_i^s + B_\lambda^* - k(w^*(x_i))\|^2 \right]^{1/2}. \\
& && \text{(definition of } \widehat{\mathcal{T}}_\lambda^{\text{lab}})
\end{aligned}$$

Picking $k(\cdot) = A_\lambda^* h^*(\cdot) + B_\lambda^*$, the above inequality becomes:

$$\begin{aligned}
\sqrt{\mathcal{L}(w^*, k^*; \mathcal{D}_t)} &\le \sqrt{\widehat{\mathcal{T}}_\lambda^{\text{lab}}(\mathcal{D}_s, \mathcal{D}_t)} + \left[\frac{1}{n} \sum_{i=1}^{n} \|A_\lambda^* [y_i^s - h^*(w^*(x_i))]\|^2 \right]^{1/2} \\
&\le \sqrt{\widehat{\mathcal{T}}_\lambda^{\text{lab}}(\mathcal{D}_s, \mathcal{D}_t)} + \|A_\lambda^*\|_F \left[\frac{1}{n} \sum_{i=1}^{n} \|y_i^s - h^*(w^*(x_i))\|^2 \right]^{1/2} \\
&= \sqrt{\widehat{\mathcal{T}}_\lambda^{\text{lab}}(\mathcal{D}_s, \mathcal{D}_t)} + \|A_\lambda^*\|_F \sqrt{\mathcal{L}(w^*, h^*; \mathcal{D}_s)}.
\end{aligned}$$

Thus, the lemma holds.

A.4 Proof of Theorem 2

Applying Lemma 2 for (w^*, k^*), with probability at least $1 - \delta$, we have:

$$\begin{aligned}
\sqrt{\mathcal{R}(w^*, k^*)} &= \sqrt{\mathcal{L}(w^*, k^*; \mathcal{D}_t) + [\mathcal{R}(w^*, k^*) - \mathcal{L}(w^*, k^*; \mathcal{D}_t)]} \\
&\le \sqrt{\mathcal{L}(w^*, k^*; \mathcal{D}_t)} + \sqrt{|\mathcal{R}(w^*, k^*) - \mathcal{L}(w^*, k^*; \mathcal{D}_t)|} \\
&\le \sqrt{\widehat{\mathcal{T}}_\lambda^{\text{lab}}(\mathcal{D}_s, \mathcal{D}_t)} + \|A_\lambda^*\|_F \sqrt{\mathcal{L}(w^*, h^*; \mathcal{D}_s)} + \sqrt{\frac{C(d, d_t, M, H, L, \delta)}{n^{1/2}}}.
\end{aligned}$$

Thus, the theorem holds.

B Additional Experiment Details and Results

B.1 More Details of the Experiment Settings

Settings for Section 5.1-5.5. In these experiments, we train our source models from scratch using the MSE loss with the AdamW optimizer (Loshchilov & Hutter, 2019), which we run for 40 epochs with batch size of 64 and the cosine learning rate scheduler. To obtain good source models, we resize all input images to 256×256 and apply basic image augmentations without horizontal flipping (i.e., affine transformation, Gaussian blur, and color jitter). We also scale all labels into $[0, 1]$ using the width and height of the input images.

For the transfer learning setting with head re-training, we freeze the trained feature extractor and re-train the regression head on the target dataset using the same setting above, except that we run 15 epochs on the CUB-200-2011 dataset and 30 epochs on the OpenMonkey dataset. For half fine-tuning, we unfreeze the last convolution layer and the head classifier since the number of trainable parameters is around half of the total number of parameters. For full fine-tuning, we unfreeze the whole network. In these two fine-tuning settings, we fine-tune for 15 epochs on both datasets. We use PyTorch (Paszke et al., 2019) for implementation.

Settings for Section 5.6. In this experiment, we use the following 8 ImageNet pre-trained models as the source models: ResNet50, ResNet101, ResNet152 (He et al., 2016), DenseNet121, DenseNet169, DenseNet201 (Huang et al., 2017), GoogleNet (Szegedy et al., 2015), and Inceptionv3 (Szegedy et al., 2016). These models are taken from the PyTorch Model Zoo.

We use the dSprites dataset (Matthey et al., 2017) for the target task. This dataset contains 737,280 images with 4 outputs for regression: x and y positions, scale, and orientation. The train-test split is similar to the settings in You et al. (2021): 60% for training, 20% for validation, and 20% for testing. The transferred MSE is computed on the test set. We train our models with 10 epochs using the AdamW optimizer. The initial learning rate is 10^{-3}, which is divided by 10 every 3 epochs.

B.2 Additional Experiment: Effects of λ

In this experiment, we investigate the effects of λ on our proposed transferability estimators. We use the setting in Section 5.2 with the CUB-200-2011 dataset and vary the value of λ in the range [0, 100] for both LabMSE and LinMSE. Table 4 reports the results for this experiment with all three transfer learning settings.

As noted in Section 5.1, adding a regularizer does not affect LabMSE much (unless λ is very large) since the labels used to compute LabMSE were already scaled to [0,1]. For head re-training, increasing λ improves the correlation for both LabMSE and LinMSE, with the best correlations achieved at $\lambda = 100$. For half fine-tuning, increasing λ slightly improves the correlation for LabMSE, but decreases the correlation for LinMSE. In this setting, LabMSE is best at $\lambda = 100$, while LinMSE is best at $\lambda = 0$. For full fine-tuning, increasing λ slightly decreases the correlations for both LabMSE and LinMSE, with the best correlations achieved at $\lambda = 0$.

We can observe from these results that varying λ does not significantly change the correlations. In the head re-training and half fine-tuning settings (where we have significant correlations for at least one transferability estimators), for **all** values of λ in Table 4, LabMSE is better than LabLogME and LabTransRate, while LinMSE is better than LogME and LabTransRate. These results show that our proposed methods are generally robust to the value of λ and also better than the baselines for a wide range of λ values.

B.3 Additional Experiment: Usefulness of Theoretical Bounds

Although the theoretical bounds in Section 3 show a relationship between the true risk of the optimal transferred model and our transferability estimators, these bounds could be loose in practice unless the number of samples is large. This is in fact a limitation of this type of generalization bounds. To show the usefulness of our bounds in practice, we conduct an experiment to investigate the generalization gap using the head re-training setting in Section 5.1. The generalization gap is defined as the *difference between our transferability score and the MSE of the transferred model*. According

Table 4: **Correlation coefficients for different values of λ** on the CUB-200-2011 dataset. Bold numbers indicate the best results in each column. Results of the baselines are given in the last 4 rows for comparison.

λ	Head re-training		Half fine-tuning		Full fine-tuning	
	LabMSE	LinMSE	LabMSE	LinMSE	LabMSE	LinMSE
0.0	0.9156	0.9205	0.5359	**0.6275**	**0.0558**	**0.0968**
0.5	0.9156	0.9316	0.5359	0.6069	**0.0558**	0.0921
1.0	0.9156	0.9317	0.5359	0.6071	**0.0558**	0.0929
2.0	0.9156	0.9321	0.5359	0.6079	**0.0558**	0.0941
5.0	0.9156	0.9331	0.5359	0.6092	**0.0558**	0.0956
7.0	0.9156	0.9336	0.5359	0.6095	0.0557	0.0959
10	0.9157	0.9342	0.5359	0.6096	0.0556	0.0961
20	0.9159	0.9358	0.5360	0.6092	0.0554	0.0959
50	0.9172	0.9380	0.5363	0.6072	0.0541	0.0948
75	0.9185	0.9391	0.5364	0.6060	0.0528	0.0943
100	**0.9198**	**0.9398**	**0.5365**	0.6051	0.0516	0.0938
LabLogME	0.547	-	0.400	-	0.120	-
LogME	-	0.889	-	0.560	-	0.099
LabTransRate	0.008	-	0.006	-	0.001	-
TransRate	-	0.029	-	0.006	-	0.100

to our theorems, this generalization gap is bounded above by the complexity term. We will compare the generalization gap with our transferability score and inspect whether it has any significant correlation with the actual transferred MSE.

From this experiment, the ratios between the transferability score and the generalization gap for our transferability estimators are: 1.6 (LinMSE0), 2.0 (LinMSE1), 2.3 (LabMSE0), and 2.3 (LabMSE1). These results show that the transferability scores dominate the generalization gap in practice. More importantly, there is *no significant correlation* between the generalization gap and the actual transferred MSE. These findings indicate that the complexity term in our bounds may have little effects for transferability estimation, as opposed to the transferability score term that has a strong effect.

B.4 Additional Experiment: Tasks with Higher Dimensional Labels

In this experiment, we further show the effectiveness of our proposed methods when the target tasks have higher dimensional labels. In particular, we transfer from 4 source tasks on CUB-200-2011 (back, beak, belly, and breast) to all the combinations of 5 attributes among the remaining tasks (except for right eye, right leg and right wing, which may not always be available in the data). In total, we have 224 source-target pairs, where the source tasks have 2-dimensional labels and the target tasks have 10-dimensional labels. We use the same training settings as in Section 5.2 and use head re-training as the transfer learning method. Figure 4 gives the results for this experiment. The figure clearly shows that our methods, LinMSE0 and LinMSE1, are both better than the LogME and TransRate baselines.

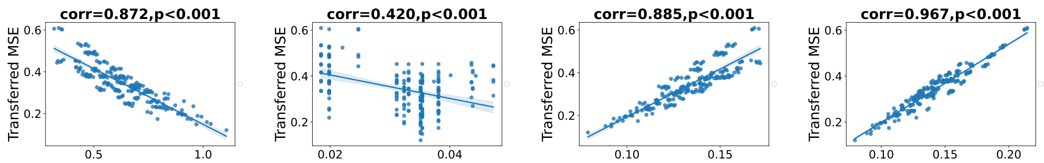

(a) LogME (2021) (b) TransRate (2022) (c) LinMSE0 (ours) (d) LinMSE1 (ours)

Figure 4: **Correlation coefficients and p-values between transferability estimators and actual test MSEs** when transferring to tasks with 10-dimensional outputs. The experiment is conducted for the head re-training setting on CUB-200-2011.

B.5 Additional Results for Section 5.1 and 5.2

Table 5: **Correlation coefficients for all source tasks** of different transferability estimators on CUB-200-2011. Bold numbers indicate the best results in each row. Asterisks (*) indicate the best results among the corresponding label-based or feature-based methods.

Transfer setting	Source task	Label-based method				Feature-based method			
		LabLogME (2021)	LabTransRate (2022)	LabMSE0 (ours)	LabMSE1 (ours)	LogME (2021)	TransRate (2022)	LinMSE0 (ours)	LinMSE1 (ours)
Head re-training	Back	0.743	0.116	**0.956***	**0.956***	0.920	0.273	0.931*	0.931*
	Beak	0.863	0.229	**0.922***	**0.922***	0.878	0.158	0.906	0.907*
	Belly	0.893	0.097	0.970*	0.970*	0.933	0.188	0.932	**0.978***
	Breast	0.914	0.119	**0.935***	**0.935***	0.903	0.279	0.922*	0.922*
	Crown	0.917	0.040	**0.962***	**0.962***	0.913	0.251	0.945	0.946*
	Forehead	0.887	0.076	**0.941***	0.940	0.885	0.221	0.924	0.925*
	Left eye	0.034	0.076	0.913*	0.913*	0.924	0.289	0.945	**0.946***
	Left leg	0.260	0.221	0.935*	0.935*	0.935	0.223	**0.953***	**0.953***
	Left wing	0.260	0.169	0.964*	0.964*	0.980	0.173	**0.994***	**0.994***
	Nape	0.888	0.084	0.922*	0.922*	0.900	0.299	**0.929***	**0.929***
	Right eye	0.625	0.242	0.904*	0.904*	0.921	0.243	**0.948***	**0.948***
	Right leg	0.507	0.047	**0.958***	**0.958***	0.942	0.217	0.954	0.956*
	Right wing	0.521	0.166	0.907*	0.907*	0.934	0.269	0.946	**0.947***
	Tail	0.591	0.392	**0.900***	**0.900***	0.872	0.544	0.880	0.881*
	Throat	0.895	0.123	**0.938***	**0.938***	0.890	0.291	0.924	0.926*
Half fine-tuning	Back	0.714	0.076	0.791*	0.791*	0.835	0.168	**0.911***	**0.911***
	Beak	0.663	0.159	0.831*	0.831*	0.765	0.076	**0.883***	**0.883***
	Belly	0.529	0.233	0.655*	0.655*	0.757	0.309	**0.849***	0.709
	Breast	0.730	0.100	0.802*	0.802*	0.762	0.152	**0.867***	**0.867***
	Crown	0.644	0.068	0.752*	0.752*	0.714	0.165	**0.832***	**0.832***
	Forehead	0.653	0.032	0.804*	0.804*	0.727	0.120	**0.859***	0.858
	Left eye	0.419	0.046	**0.913***	**0.913***	0.812	0.227	0.892*	0.891
	Left leg	0.120	0.094	0.721*	0.721*	0.845	0.150	**0.893***	**0.893***
	Left wing	0.352	0.149	**0.949***	**0.949***	0.859	0.189	0.919*	0.919*
	Nape	0.660	0.055	0.705*	0.705*	0.751	0.181	**0.863***	**0.863***
	Right eye	0.561	0.221	**0.911***	**0.911***	0.786	0.180	0.871*	0.871*
	Right leg	0.267	0.125	0.690*	0.690*	0.810	0.069	**0.861***	0.858
	Right wing	0.407	0.133	0.495*	0.495*	0.515	0.338	0.521	**0.522***
	Tail	0.800	0.117	**0.929***	**0.929***	0.847	0.285	0.924*	0.924*
	Throat	0.767	0.012	0.869*	0.869*	0.811	0.253	**0.900***	0.898
Full fine-tuning	Back	0.710	0.085	0.785*	0.785*	0.829	0.178	**0.906***	**0.906***
	Beak	0.659	0.161	0.826*	0.826*	0.758	0.073	**0.877***	**0.877***
	Belly	0.645	0.273	0.782*	0.782*	0.861	0.365	**0.926***	0.826
	Breast	0.740	0.104	0.811*	0.811*	0.768	0.152	**0.871***	**0.871***
	Crown	0.647	0.073	0.756*	0.756*	0.717	0.157	**0.834***	0.833
	Forehead	0.648	0.037	0.799*	0.799*	0.723	0.111	**0.855***	0.854
	Left eye	0.224	**0.456***	0.297	0.297	0.333*	0.246	0.282	0.284
	Left leg	0.057	0.067	0.659*	0.659*	0.796	0.146	**0.850***	**0.850***
	Left wing	0.342	0.159	**0.954***	**0.954***	0.860	0.195	0.920*	0.920*
	Nape	0.667	0.041	0.713*	0.713*	0.752	0.177	**0.864***	**0.864***
	Right eye	0.549	0.213	**0.915***	**0.915***	0.794	0.199	0.877*	0.877*
	Right leg	0.237	0.377	0.673*	0.673*	0.755	0.431	**0.766***	0.763
	Right wing	**0.254***	0.046	0.237	0.237	0.225	0.093	0.227*	0.226
	Tail	0.803	0.122	**0.930***	**0.930***	0.846	0.288	0.923*	0.923*
	Throat	0.665	0.027	0.801*	0.801*	0.744	0.256	**0.850***	0.848

Table 6: **Correlation coefficients for all source tasks** of different transferability estimators on OpenMonkey. Bold numbers indicate the best results in each row. Asterisks (*) indicate the best results among the corresponding label-based or feature-based methods.

Transfer setting	Source task	Label-based method				Feature-based method			
		LabLogME (2021)	LabTransRate (2022)	LabMSE0 (ours)	LabMSE1 (ours)	LogME (2021)	TransRate (2022)	LinMSE0 (ours)	LinMSE1 (ours)
Head re-training	Right eye	0.894	0.859	0.986*	0.986*	0.992	0.846	0.979	**0.994***
	Left eye	0.895	0.854	0.987*	0.987*	0.915	0.858	0.982	**0.995***
	Nose	0.908	0.849	0.988*	0.988*	0.856	0.837	0.979	**0.996***
	Head	0.941	0.881	0.992*	0.992*	0.872	0.884	0.984	**0.994***
	Neck	0.972	0.862	**0.998***	**0.998***	0.960	0.839	0.984	0.997*
	Right shoulder	0.977	0.837	0.994*	0.994*	0.955	0.811	0.983	**0.995***
	Right elbow	0.963	0.529	0.994*	0.994*	0.890	0.564	0.974	**0.996***
	Right wrist	0.970	0.753	0.993*	0.993*	0.614	0.446	0.969	**0.995***
	Left shoulder	0.972	0.800	0.997*	0.997*	0.772	0.808	0.989	**0.999***
	Left elbow	0.960	0.546	0.994*	0.994*	0.256	0.572	0.972	**0.998***
	Left wrist	0.975	0.597	0.993*	0.993*	0.689	0.544	0.966	**0.996***
	Hip	0.922	0.540	0.988*	0.988*	0.881	0.557	0.817	**0.992***
	Right knee	0.925	0.080	0.975*	0.975*	0.919	0.331	0.949	**0.984***
	Right ankle	0.931	0.411	0.989*	0.989*	0.538	0.371	0.935	**0.993***
	Left knee	0.923	0.160	0.978*	0.978*	0.936	0.209	0.939	**0.990***
	Left ankle	0.916	0.416	0.986*	0.986*	0.8737	0.329	0.928	**0.993***
	Tail	0.936	0.712	**0.993***	**0.993***	0.625	0.662	0.892	0.990*
Half fine-tuning	Right eye	0.795	0.734	0.906*	0.906*	0.772	0.709	**0.960***	0.923
	Left eye	0.797	0.731	0.905*	0.905*	0.789	0.719	**0.959***	0.918
	Nose	0.829	0.736	0.914*	0.914*	0.739	0.721	**0.966***	0.926
	Head	0.835	0.759	0.921*	0.921*	0.754	0.751	**0.962***	0.930
	Neck	0.902	0.793	0.929*	0.929*	0.816	0.765	**0.967***	0.934
	Right shoulder	0.887	0.725	0.924*	0.924*	0.853	0.758	**0.970***	0.932
	Right elbow	0.764	0.250	0.806*	0.806*	0.621	0.602	**0.924***	0.833
	Right wrist	0.806	0.501	0.823*	0.823*	0.209	0.643	**0.920***	0.840
	Left shoulder	0.893	0.718	0.927*	0.927*	0.731	0.774	**0.971***	0.937
	Left elbow	0.782	0.369	0.824*	0.824*	0.153	0.594	**0.943***	0.845
	Left wrist	0.822	0.523	0.828*	0.828*	0.401	0.663	**0.924***	0.839
	Hip	0.030	0.487*	0.233	0.233	0.159	0.359	**0.782***	0.346
	Right knee	0.481	0.429	0.598*	0.598*	0.421	0.067	**0.820***	0.631
	Right ankle	0.357	0.275	0.534*	0.534*	0.019	0.226	**0.797***	0.577
	Left knee	0.467	0.355	0.601*	0.601*	0.491	0.215	**0.846***	0.658
	Left ankle	0.331	0.242	0.530*	0.530*	**0.816***	0.572	0.189	0.303
	Tail	0.231	0.196	0.434*	0.434*	0.335	0.212	**0.638***	0.342
Full fine-tuning	Right eye	0.796	0.711	0.905*	0.905*	0.754	0.693	**0.957***	0.922
	Left eye	0.790	0.733	0.904*	0.904*	0.780	0.713	**0.956***	0.918
	Nose	0.810	0.731	0.911*	0.911*	0.722	0.708	**0.958***	0.928
	Head	0.801	0.737	0.899*	0.899*	0.712	0.718	**0.945***	0.912
	Neck	0.893	0.781	0.930*	0.930*	0.818	0.743	**0.960***	0.934
	Right shoulder	0.896	0.721	**0.992***	0.936	0.865	0.750	0.973*	0.944
	Right elbow	0.689	0.168	0.736*	0.736*	0.549	0.562	**0.880***	0.769
	Right wrist	0.795	0.505	0.805*	0.805*	0.194	0.644	**0.900***	0.822
	Left shoulder	0.872	0.690	0.901*	0.901*	0.212	0.537	**0.910***	0.798
	Left elbow	0.726	0.282	0.774*	0.774*	0.395	0.672	**0.894***	0.798
	Left wrist	0.786	0.487	**0.983***	0.786	0.125	0.382	0.736*	0.284
	Hip	0.016	0.518*	0.173	0.173	0.336	0.141	**0.750***	0.550
	Right knee	0.391	0.518*	0.516	0.516	0.025	0.340	**0.715***	0.481
	Right ankle	0.246	0.396	0.436*	0.436*	**0.981***	0.722	0.977	0.977
	Left knee	0.381	0.338	0.521*	0.521*	0.405	0.303	**0.779***	0.582
	Left ankle	0.244	0.297	0.444*	0.444*	0.100	0.357	**0.744***	0.486
	Tail	0.105	0.299	0.309*	0.309*	0.335	0.212	**0.638***	0.341

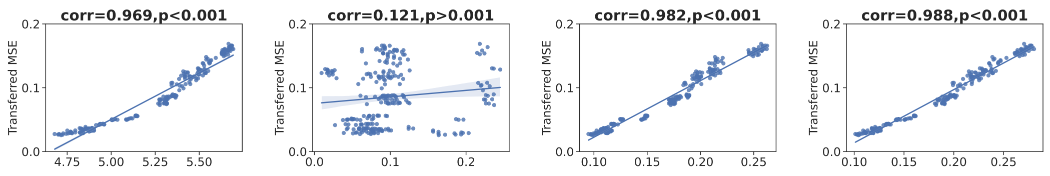

(a) LogME (2021) (b) TransRate (2022) (c) LinMSE0 (ours) (d) LinMSE1 (ours)

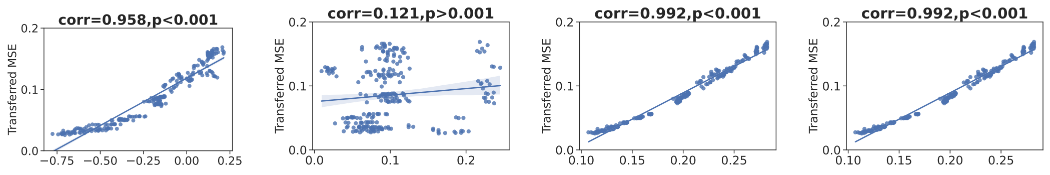

(e) LabLogME (2021) (f) LabTransRate (2022) (g) LabMSE0 (ours) (h) LabMSE1 (ours)

Figure 5: **Correlation coefficients and p-values between transferability estimators and actual test MSEs** when transferring with head re-training from OpenMonkey to CUB-200-2011.

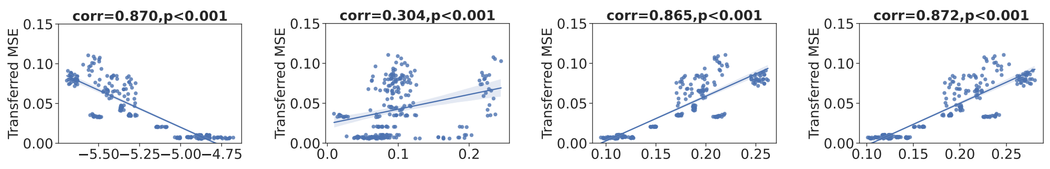

(a) LogME (2021) (b) TransRate (2022) (c) LinMSE0 (ours) (d) LinMSE1 (ours)

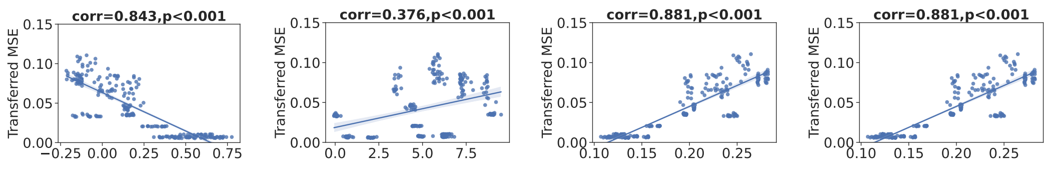

(e) LabLogME (2021) (f) LabTransRate (2022) (g) LabMSE0 (ours) (h) LabMSE1 (ours)

Figure 6: **Correlation coefficients and p-values between transferability estimators and actual test MSEs** when transferring with half fine-tuning from OpenMonkey to CUB-200-2011.

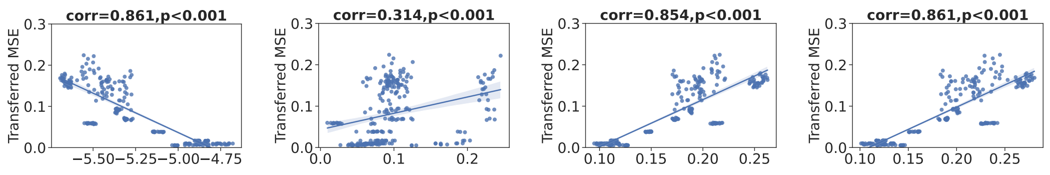

(a) LogME (2021) (b) TransRate (2022) (c) LinMSE0 (ours) (d) LinMSE1 (ours)

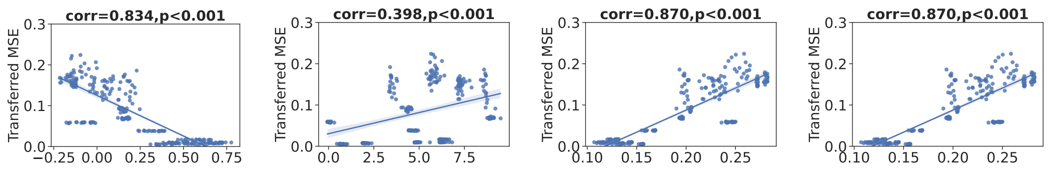

(e) LabLogME (2021) (f) LabTransRate (2022) (g) LabMSE0 (ours) (h) LabMSE1 (ours)

Figure 7: **Correlation coefficients and p-values between transferability estimators and actual test MSEs** when transferring with full fine-tuning from OpenMonkey to CUB-200-2011.

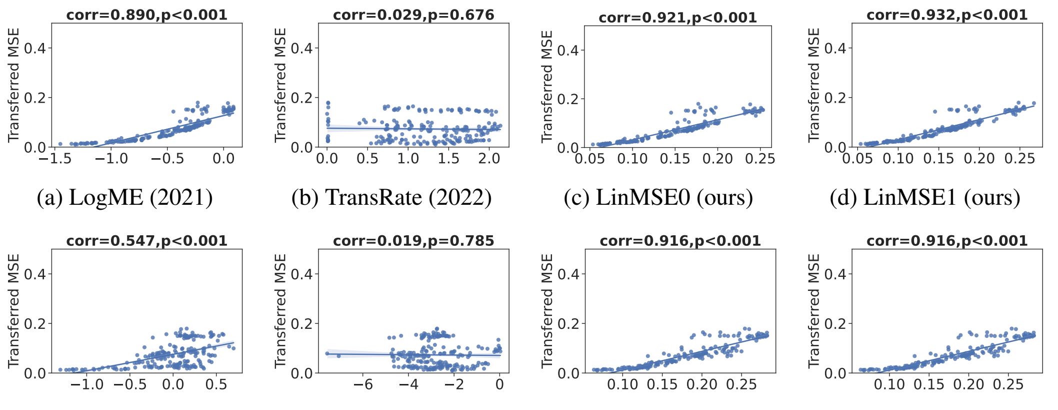

(a) LogME (2021) (b) TransRate (2022) (c) LinMSE0 (ours) (d) LinMSE1 (ours)
(e) LabLogME (2021) (f) LabTransRate (2022) (g) LabMSE0 (ours) (h) LabMSE1 (ours)

Figure 8: **Correlation coefficients and p-values between transferability estimators and actual test MSEs** when transferring with head re-training between any two different keypoints (with shared inputs) on CUB-200-2011.

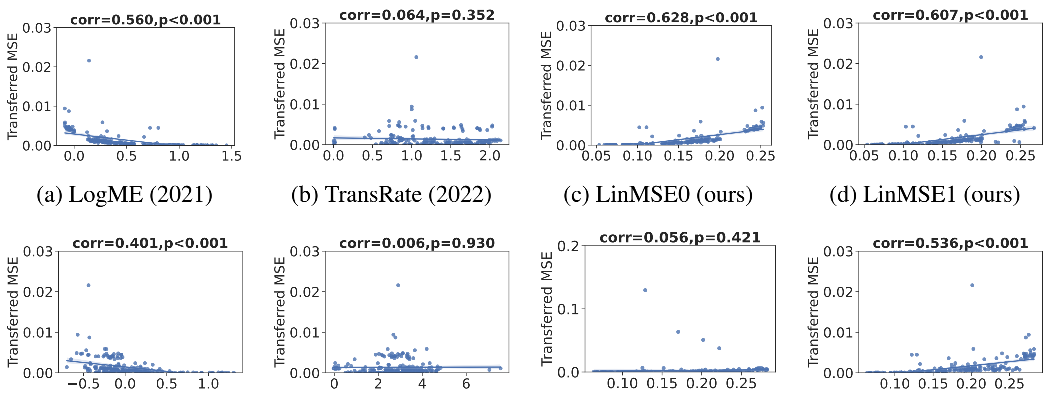

(a) LogME (2021) (b) TransRate (2022) (c) LinMSE0 (ours) (d) LinMSE1 (ours)
(e) LabLogME (2021) (f) LabTransRate (2022) (g) LabMSE0 (ours) (h) LabMSE1 (ours)

Figure 9: **Correlation coefficients and p-values between transferability estimators and actual test MSEs** when transferring with half fine-tuning between any two different keypoints (with shared inputs) on CUB-200-2011.

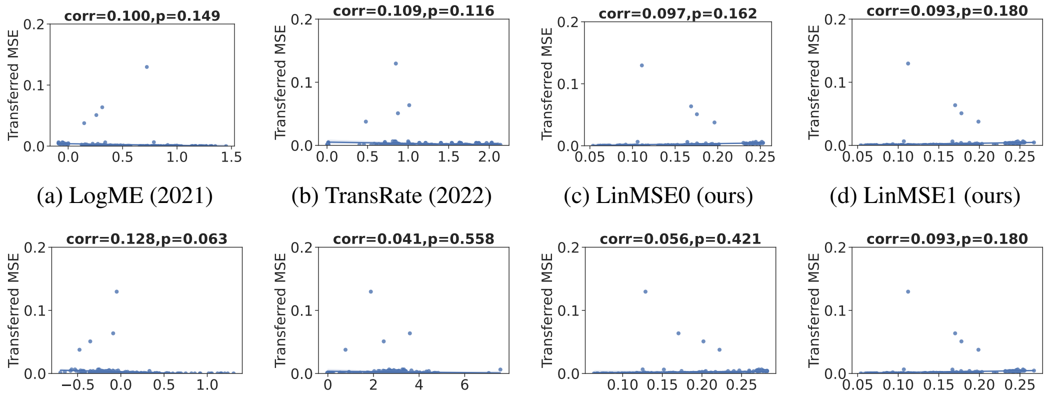

(a) LogME (2021) (b) TransRate (2022) (c) LinMSE0 (ours) (d) LinMSE1 (ours)
(e) LabLogME (2021) (f) LabTransRate (2022) (g) LabMSE0 (ours) (h) LabMSE1 (ours)

Figure 10: **Correlation coefficients and p-values between transferability estimators and actual test MSEs** when transferring with full fine-tuning between any two different keypoints (with shared inputs) on CUB-200-2011.

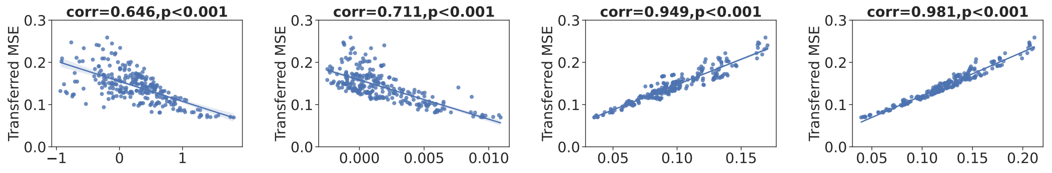

(a) LogME (2021) (b) TransRate (2022) (c) LinMSE0 (ours) (d) LinMSE1 (ours)

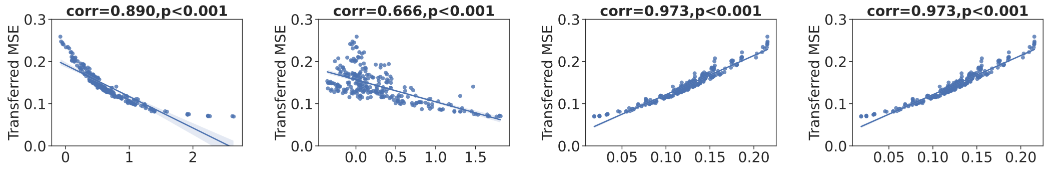

(e) LabLogME (2021) (f) LabTransRate (2022) (g) LabMSE0 (ours) (h) LabMSE1 (ours)

Figure 11: **Correlation coefficients and p-values between transferability estimators and actual test MSEs** when transferring with head re-training between any two different keypoints (with shared inputs) on OpenMonkey.

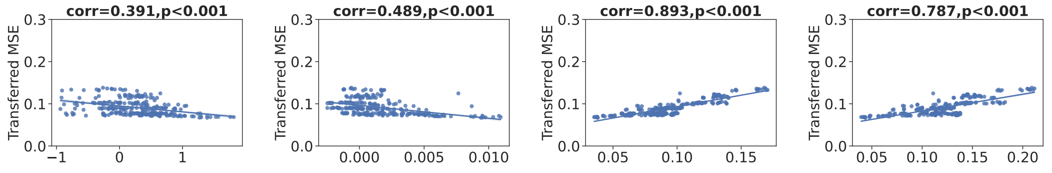

(a) LogME (2021) (b) TransRate (2022) (c) LinMSE0 (ours) (d) LinMSE1 (ours)

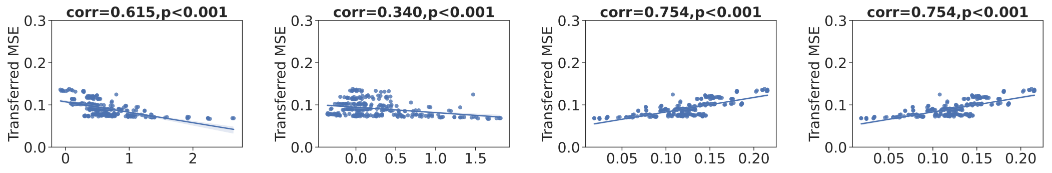

(e) LabLogME (2021) (f) LabTransRate (2022) (g) LabMSE0 (ours) (h) LabMSE1 (ours)

Figure 12: **Correlation coefficients and p-values between transferability estimators and actual test MSEs** when transferring with half fine-tuning between any two different keypoints (with shared inputs) on OpenMonkey.

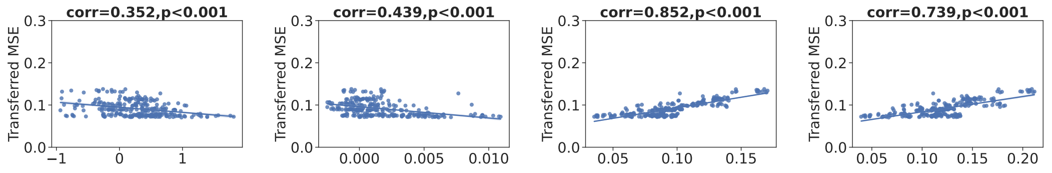

(a) LogME (2021) (b) TransRate (2022) (c) LinMSE0 (ours) (d) LinMSE1 (ours)

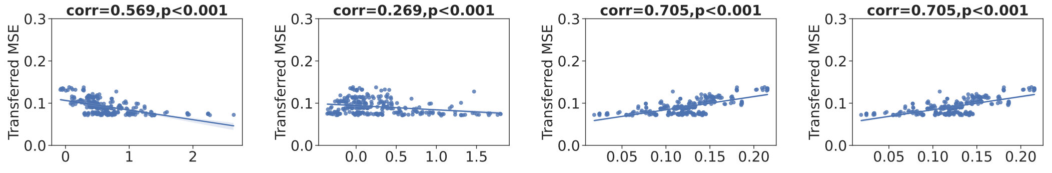

(e) LabLogME (2021) (f) LabTransRate (2022) (g) LabMSE0 (ours) (h) LabMSE1 (ours)

Figure 13: **Correlation coefficients and p-values between transferability estimators and actual test MSEs** when transferring with full fine-tuning between any two different keypoints (with shared inputs) on OpenMonkey.